Formation of Electric Potential during the Oxidation of a Metal Particle

Igor Filimonov and Dan Luss
Dept. of Chemical Engineering, University of Houston, Houston, TX 77204-4792

DOI 10.1002/aic.10195
Published online in Wiley InterScience (www.interscience.wiley.com).

Experiments revealed that a transient electric voltage of the order of 1 V may form during the combustion of a single metal particle. We present a model showing that such an electrical field may form as a result of the different diffusion rates of the positive and negative charge carriers through a growing mixed-ionic-electronic-conducting oxide shell. Simulations of the evolution of the electric charge carriers and temporal potential distribution reveal that three key parameters affect the voltage formation. The ratio of the characteristic oxygen ion diffusion rate within the particle to the maximum oxygen transport rate to the particle surface affects the formation of a diffusion layer and the carrier distributions inside the oxide shell. The ratio between the thickness of an exterior oxide layer, formed before the reaction has started, and the Debye screening length has a strong impact on the amplitude and temporal evolution of the voltage. The thinner this initial oxide shell is, the larger is the voltage amplitude. The ratio between the diffusion coefficients of the positive and negative charge carriers determines the sign of the excess electrical charge on the surface. © 2004 American Institute of Chemical Engineers *AIChE J,* 50: 2287–2296, 2004

Keywords: mixed-ionic-electronic-conducting (MIEC) oxide shell, electric charge carrier, diffusion, oxygen transport rate, Debye screening length

Introduction

Recent experimental investigations (Kudryashov et al., 1997; Martirosyan et al., 2003a,b; Morozov et al., 1997; Nersesyan et al., 2002) have revealed that a moving solid (solid–gas) combustion wave may generate an electromagnetic impulse in and around the solid. Electrical impulse with an amplitude of up to about 1 V and magnetic fields of micro-Teslas were observed by Nersesyan et al. (2002) and Martirosyan et al. (2003a,b) during the high-temperature oxidation of various metals. The mechanism generating the electrical impulse is not yet understood.

Theoretical studies predicted that external Joule heating could sustain the combustion when the adiabatic temperature was too low to maintain a moving reaction front (Feng and Munir, 1995; Filimonov and Kidin, 1992, 1996; Kidin and Filimonov, 1990, 1992; Munir, 2000; Zakiev, 1999). This prediction was verified experimentally (Dalton et al., 1990; Maglia et al., 2001; Munir, 2000; Trofimov and Yukhvid, 1993). However, these models of solid combustion did not account for the electromagnetic impulse produced by the moving temperature wave.

The electromagnetic impulse generated during solid (solid–gas) combustion cannot be predicted by the existing pseudo-homogeneous models of reactive solid powder. The experimental findings strongly suggest that the combustion process should be considered on the level of a single particle (Martirosyan et al., 2003a). This generation of an electromagnetic field is of both intrinsic scientific interest and of potential practical importance. Therefore, it is important to develop an understanding and ability to predict this phenomenon and its impact.

Metal particle oxidation may proceed in two ways, depend-

Permanent address of I. Filimonov: Institute of Structural Macrokinetics and Materials Science, RAS, Chernogolovka 142432, Russia.
Correspondence concerning this article should be addressed to D. Luss at dluss@uh.edu.

ing on the metal properties and oxygen pressure. Metal cations (and/or their vacancies) may diffuse and become oxidized at the particle surface [such as Fe oxidation (Kofstad, 1988)], or oxygen ions (and/or their vacancies) may diffuse to and react at the metal–oxide interface [such as Zr oxidation (Gellings and Bouwmeester, 1997)]. The oxidation of some metals, such as Ti, may occur either on the particle surface or on the metal–oxide interface, depending on operating conditions (Kofstad, 1988; Rode et al., 1992, 1995). We consider here the case in which the oxide is a mixed-ionic-electronic-conductor (MIEC) and the oxidation occurs on the metal–oxide interface. Rode et al. (1992) used simplified transport relations to investigate the case in which the oxide is an n-type semiconductor and the reaction between metal cations and electrons occurs on the particle surface. The emphasis of their study was on self-heating rather than the evolution of the electrical field.

Our model assumes that an electrical field is generated as a result of the formation of a double-charge layer by the diffusion of charge carriers through a growing MIEC oxide shell. As a first step we consider the voltage generation under isothermal conditions. This simplification decreases the number of parameters in the mathematical model and provides insight into the impact of various rate processes and parameters on the electrical field formation. The impact of the temperature increase during the exothermic reaction will be examined in a future publication. Understanding the behavior of a single pellet is a starting point for a model predicting the electrical field formation during metal powder combustion.

Development of a Mathematical Model

We consider the isothermal oxidation of a spherical metal pellet of radius R_0 with a thin exterior oxide shell, which formed before the start of the reaction. After a rapid initial heating (ignition) a very fast metal oxidation starts in accordance with the shrinking core model (Levenspiel, 1962; Wen, 1968). Positive and negative charge carriers form on the pellet surface after ambient oxygen adsorption and incorporation into the atomic lattice of the oxide. The oxygen ions (and/or their vacancies) diffuse toward the shrinking metal core through the MIEC shell. The different rates of diffusion of the positive and negative charge carriers generate an electric potential gradient in the growing oxide shell. We consider the same surface reactions as those in published models of oxygen permeation through MIEC membranes. Unlike these models, we do not assume a local electrochemical (chemical) equilibrium or electrical charge neutrality.

We assume that ambient gaseous oxygen is adsorbed in a very thin layer on the pellet surface by the reversible reaction

$$\frac{1}{2}\,O_2(g) \underset{K'_{-1}}{\overset{K_1}{\rightleftharpoons}} O_{ads} \tag{1}$$

The adsorbed oxygen forms interstitial ions and vacancies by the reactions

$$V_O^{++} + 2e^- + O_{ads} \underset{K'_{-2}}{\overset{K'_2}{\rightleftharpoons}} O^{\times} \underset{K'_{-3}}{\overset{K'_3}{\rightleftharpoons}} V_O^{++} + O^{2-} \tag{2}$$

Simultaneously, electron-hole pairs are generated by thermal ionization

$$\text{nil} \underset{K'_{-4}}{\overset{K'_4}{\rightleftharpoons}} e^- + h^+ \tag{3}$$

The diffusion coefficients (D_i) of the charge carriers (V_O^{++}, $e-$, O^{2-}, and h^+) in the growing oxide shell have different values. The oxygen ions are consumed by a very fast, irreversible reaction at the shrinking metal core of radius R_{ox}

$$\nu Me + 2O^{2-} + 4h^+ \rightarrow Me_\nu O_2 \tag{4}$$

The reaction network (Eqs. 1–3) is a generalization of those described by Chandra (1981), Dou et al. (1985), Ramanarayanan et al. (1991), Lin et al. (1994), and Gellings and Bouwmeester (1997). The rates of reactions 1–3 satisfy the following relations

$$W_1 = -\frac{1}{2}\frac{d[O_{2,g}]}{dt} = K_1[O_{2,g}]^{1/2} - K'_{-1}[O_{ads}] \tag{5}$$

$$W_2 = \frac{d[O^{\times}]}{dt} = -\frac{d[V_O^{++}]}{dt} = K'_2[V_O^{++}][e^-]^2[O_{ads}] - K'_{-2}[O^{\times}] - K'_3[O^{\times}] + K'_{-3}[V_O^{++}][O^{2-}] \tag{6}$$

$$W_3 = \frac{d[O^{2-}]}{dt} = K'_3[O^{\times}] - K'_{-3}[V_O^{++}][O^{2-}] \tag{7}$$

$$W_4 = -\frac{d[h^+]}{dt} = K'_4 - K'_{-4}[e^-][h^+] \tag{8}$$

The lattice oxygen concentration $[O^{\times}]$, in the MIEC shell, may be considered to be a constant (Gellings and Bouwmeester, 1997; Lin et al., 1994). In addition, we assume that the concentration of the interstitial oxygen ions (O^{2-}) and electron holes (h^+) attain a quasi-steady state, that is

$$W_i = 0 \qquad i = 2,\ 3,\ 4 \tag{9}$$

The oxygen concentration near the pellet surface $[O_{2,g}]$ satisfies the relation

$$k_c([O_{2,g}]^{\infty} - [O_{2,g}]) = W_1 \tag{10}$$

where k_c is the mass transfer coefficient and $[O_{2,g}]^{\infty}$ is the ambient oxygen concentration.

At high oxygen pressures interstitial oxygen ions (O^{2-}) and electron holes (h^+) are the main contributors to oxygen and charge transport in MIEC materials (Chandra 1981; Gellings and Bouwmeester, 1997; Lin et al., 1994). Equations 6–9 indicate that in this case

$$[O_{ads}] = \frac{K_{-1}}{K'_{-1}}[O^{2-}][h^+]^2 \qquad K_{-1} = K'_{-1}\left(\frac{K'_{-2}}{K'_2}\right)\left(\frac{K'_{-3}}{K'_3}\right)\left(\frac{K'_{-4}}{K'_4}\right)^2 \tag{11}$$

The electrochemical equilibrium concentrations of reactions 1–3 are

$$[O^{2-}]^* = \left(\frac{K_1}{4K_{-1}}\right)^{1/3}([O_{2,g}]^\infty)^{1/6}$$

$$[h^+]^* = \left(\frac{2K_1}{K_{-1}}\right)^{1/3}([O_{2,g}]^\infty)^{1/6} \tag{12}$$

At low oxygen pressures oxygen ion vacancies (V_O^{++}) and electrons (e^-) provide oxygen permeation through the membranes and

$$[O_{ads}] = \frac{\tilde{K}_{-1}}{K'_{-1}}[V_O^{++}]^{-1}[e^-]^{-2} \qquad \tilde{K}_{-1} = K'_{-1}\left(\frac{K'_{-2}}{K'_2}\right)[O^\times] \tag{13}$$

The electrochemical equilibrium concentrations of reactions 1–3 in this case are

$$[V^{++}]^* = \left(\frac{\tilde{K}_{-1}}{4K_1}\right)^{1/3}([O_{2,g}]^\infty)^{-1/6}$$

$$[e^-]^* = \left(\frac{2\tilde{K}_{-1}}{K_1}\right)^{1/3}([O_{2,g}]^\infty)^{-1/6} \tag{14}$$

Our model is for operation when $[O_{2,g}]^\infty \gg K_{-1}\tilde{K}_{-1}/K_1^2$, that is

$$[O^{2-}]^* \gg [V_O^{++}]^* \qquad [h^+] \gg [e^-]^* \tag{15}$$

At low oxygen concentrations the inverse of inequality 15 is valid. At intermediate oxygen concentrations, the model has to account for all four charge carriers (oxygen ions, vacancies, holes, and electrons). By solving Eqs. 5, 10, and 11 we obtain

$$y = \frac{A^2}{4}\left[\left(1 + \frac{4}{A^2} + \frac{4np^2}{A}\right)^{1/2} - 1\right]^2 \tag{16}$$

where

$$y = [O_{2,g}]/[O_{2,g}]^\infty \qquad n = [O^{2-}]/[O^{2-}]^*$$

$$p = [h^+]/[h^+]^* \qquad A = \frac{K_1}{k_c([O_{2,g}]^\infty)^{1/2}} \tag{17}$$

Thus, no oxygen adsorption occurs ($y \to 1$) either at low-temperatures ($A \to 0$) or when the reaction is completed ($n \to 1$, $p \to 1$).

The production rate of ions and holes equals their diffusive flux from the surface into the oxide shell. The nondimensional boundary conditions are

$$\beta(\nabla_\xi n - 2n\nabla_\xi\phi)_{\xi=1} = 1 - y \qquad \xi = 1 \tag{18}$$

$$\bar{D}\cdot\beta(\nabla_\xi p + p\nabla_\xi\phi)_{\xi=1} = 1 - y \qquad \xi = 1 \tag{19}$$

where

$$\bar{D} = D_+/D_- \qquad \xi = r/R_0 \qquad \phi = e\varphi/kT_0$$

$$\beta = \left(\frac{D_-[O^{2-}]^*}{2R_0}\right)/(k_c[O_{2,g}]^\infty) \tag{20}$$

The electric potential distribution satisfies the Poisson equation

$$\Lambda^2\cdot\Delta_{\xi\xi}\phi - n + p = 0 \qquad \Lambda = \left\langle\frac{kT_0}{4\pi\cdot e^2}\frac{1}{R_0^2}\frac{1}{[h^+]^*N_A}\right\rangle^{1/2} \tag{21}$$

The evolution of the charge carrier distributions within the oxide shell obeys the transient diffusion equations, as follows

$$\frac{\partial n}{\partial\tau} = \nabla_\xi^2 n - 2\nabla_\xi(n\nabla_\xi\phi) \tag{22}$$

$$\frac{\partial p}{\partial\tau} = \bar{D}\cdot[\nabla_\xi^2 p + \nabla_\xi(p\nabla_\xi\phi)] \tag{23}$$

where

$$\tau = t/t_- \qquad t_- = R_0^2/D_- \tag{24}$$

The steady-state version of Eqs. 21–23 is the Poisson–Nernst–Plank set of equations (Barcilon et al., 1997; Jerome, 1985; Park et al., 1997).

The pellet electric potential within the shrinking core is uniform because of the high metal conductivity. Thus

$$\left(\frac{\partial\phi}{\partial\xi}\right) = 0 \qquad \xi = \xi_{ox} \tag{25}$$

Because of charge conservation the particle surface boundary condition is

$$\left(\frac{\partial\phi}{\partial\xi}\right) = p - n \qquad \xi = 1 \tag{26}$$

The charge carriers arriving at the shrinking metal core (metal–oxide interface) are consumed by a very fast, irreversible reaction, that is

$$n = p = 0 \qquad \xi = \xi_{ox} > 0 \tag{27}$$

When all the metal has been oxidized, this boundary condition becomes

$$\frac{\partial n}{\partial\xi} = \frac{\partial p}{\partial\xi} = 0 \qquad \xi \equiv 0 \tag{28}$$

The molar consumption rate of the metal equals $\nu/2$ of that of the oxygen ions. Thus

$$\frac{d\xi_{ox}}{d\tau} = -I \cdot \beta(\nabla_{\xi} n - 2n\nabla_{\xi}\phi)_{\xi=\xi_{ox}} \qquad I = \frac{\nu}{2}\frac{M_W}{\rho}[O_{2,g}]^{\infty}\left(\frac{2k_c R_0}{D_-}\right) \tag{29}$$

The model consists of Eqs. 21–23, subject to boundary conditions 18, 19, 27, or 28 for the carrier concentrations and 25 and 26 for the electric potential. The corresponding initial conditions are

$$n = p = \phi \equiv 0 \qquad \tau = 0 \qquad \forall\ \xi \tag{30}$$

The movement of the shrinking metal core is described by Eq. 29.

Using the relaxation technique (Press et al., 1993) we treat the elliptic Eq. 21 as a parabolic one. The differential Eqs. 21–23 were transformed into a tridiagonal set of linear algebraic equations, which were solved by the Thomas algorithm (Ames, 1977; Thomas, 1949) with a uniform grid of 500 node points.

Behavioral Features of the Model

The simulations indicate that the evolution of the electric potential and the carrier distributions are most strongly affected by three parameters: $\bar{D}$, β, and $(1 - \xi^0_{ox})/\Lambda$. The ratio between the diffusion coefficients of the two charge carriers for three metals and two oxides, based on values reported by Mrowec (1980), Kofstad, (1988), Shelby (1996), and Grigoriev and Melikhov (1997), is illustrated in Figure 1. It shows that the $\bar{D}$ ratio can vary over a very wide range of approximately (10^{-5}, 10^3) and strongly depends on the metal and temperature. We carried out numerical simulations for ΛR_0 in the range of ($10^{-2} \div 10^{-1}$)R_0. We assume that a thin oxide layer formed before the combustion started and use in all the simulations $I = 21.3$ and $A = 1.99$.

Figures 2–4 describe the influence of $\bar{D}$ and β on the carrier and electric potential distributions during the oxidation of a single pellet with an initial oxide shell much thinner than the Debye screening length [that is, $(1 - \xi^0_{ox}) \ll \Lambda$]. When $\bar{D}$ exceeds unity, initially the diffusive flux of positive charge carriers from the surface toward the shrinking core is larger than that of the negative ones. Thus, the surface concentration of the negative charge carriers exceeds that of positive ones close to the surface. The inverse occurs when $\bar{D} < 1$ (Figures 2A and B). The difference between the surface charges, which rapidly decreases, determines the sign of the electrical potential. A negative (positive) electrical potential develops for $\bar{D} > 1$ ($\bar{D} < 1$) (Figure 3A). The larger the value of $|\bar{D} - 1|$, the larger the amplitude of the electric signal. When the two diffusion coefficients are equal no electric field develops in the pellet. There is no effect of $\bar{D}$ on the carrier concentrations after the initial period (Figures 2C and 3B). After a very short time n and p are almost indistinguishable and we show only the n profiles for these cases (Figure 2C).

Figures 2 and 3 represent cases in which the characteristic molar fluxes of both the negative and positive charge carriers are large (that is, $\beta \to 1$ and $\bar{D}\beta \gtrless 1$). The positive and negative charge profiles are almost identical throughout the pellet so that the electrical charge in the shrinking metal core and in most of the oxide shell is negligibly small. Very small

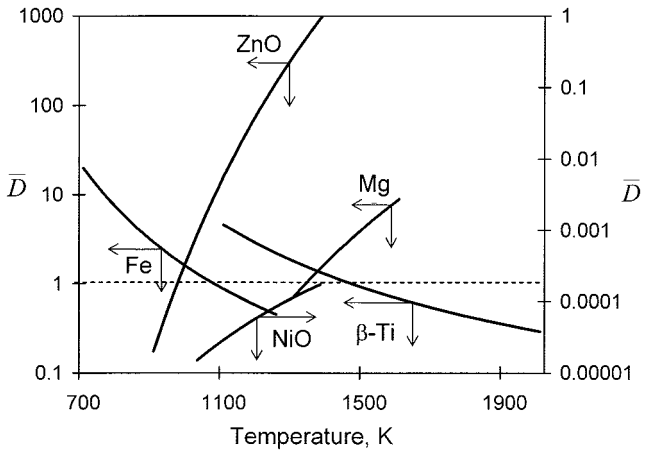

Figure 1. Dependency of $\bar{D}$ on the temperature and composition of several metals and oxides.

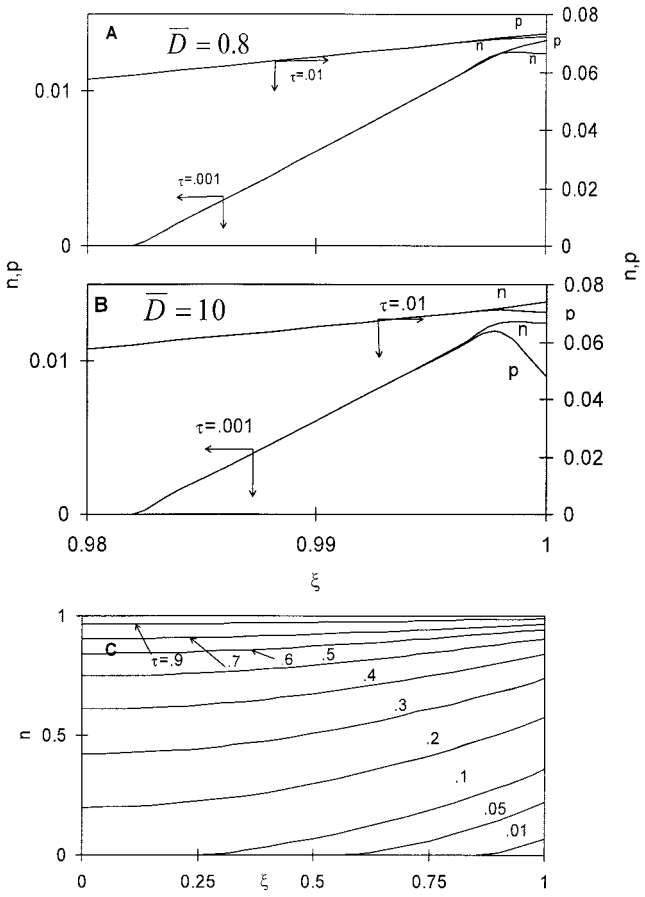

Figure 2. Temporal spatial distribution of the charge carriers during the initial stage of combustion for $\bar{D}$ = 0.8 (A) and $\bar{D}$ (B).

At the later combustion stage the distributions for $\bar{D}$values of 0.8 and 10 are indistinguishable (C). In all these simulations $\Lambda = 0.1$, $\xi^0_{ox} = 0.996$, and $\beta = 0.95$.

differences exist between the carrier concentrations at the surface and the metal–oxide interface, $n(1) - n(i) \approx n(1) \ll 1$, $p(1) - p(i) \approx p(1) \ll 1$ (that is, a diffusion layer does not form), and the carrier distributions are slightly convex (Figures 2A–C). A noticeable difference between p and n exists just close to the pellet surface at $\tau \ll 1$. The larger the magnitude of $|\bar{D} - 1|$, the larger is this difference (Figures 2A and B).

The carrier concentrations on the surface and interface increase slowly at large β values and reach equilibrium shortly before the combustion is completed (Figure 3B). The slow buildup of the surface (and interface) carrier concentrations decreases the difference between them and creates a small and slowly growing electric potential (Figure 3A).

Figure 4 describes a case in which the characteristic molar fluxes of the charge carriers are rather small (that is, $\bar{D}\beta \ll 1$ and $\beta \ll 1$). A very thin diffusion layer, in which $n(1) - n(i) \approx O(1)$ and $p(1) - p(i) \approx O(1)$, forms initially (Figure 4A). The difference between the negative and positive carrier concentrations is similar to that in the case of large β values. After the initial period, the concentrations are essentially identical and independent of $\bar{D}$ and depend mainly on the β values (Figures 2C and 4B). When β is small the carrier surface concentrations rapidly reach equilibrium. Thus, a large difference exists between the carrier concentration at the surface and the shrinking core during most of the combustion (Figures 4B and C).

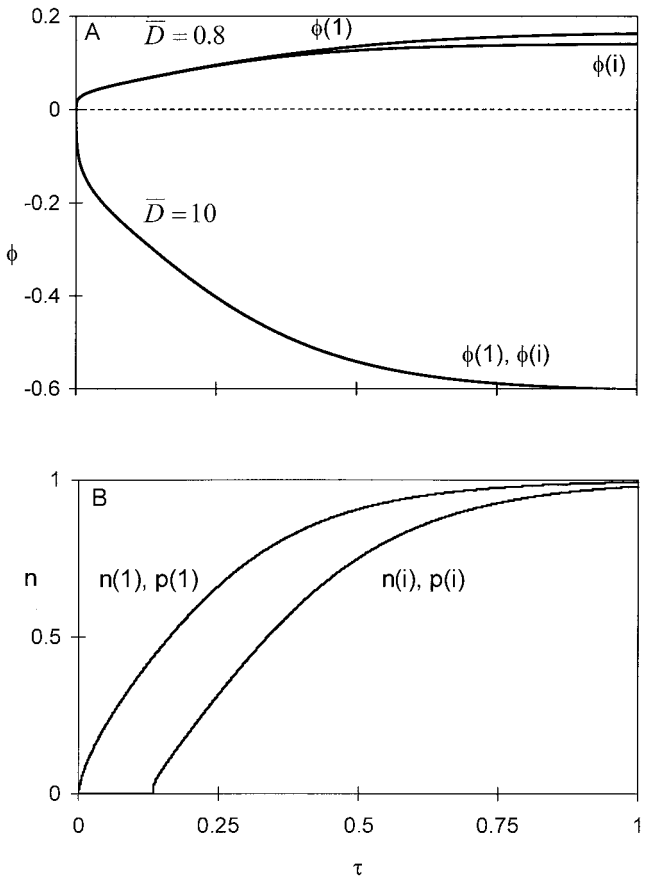

Figure 3. Effect of $\bar{D}$ on the surface and metal–oxide interface electric potential (A) and carrier concentrations for $\bar{D}$ values of 10 and 0.8 (B).

Same parameters as in Figure 2.

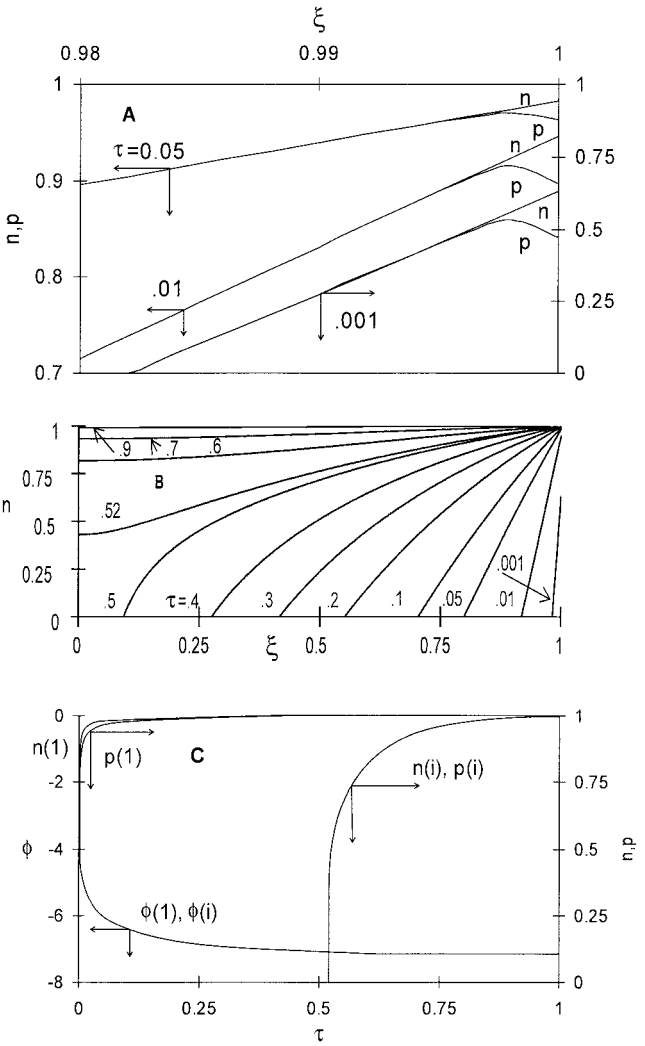

Figure 4. Spatial carrier distributions during the initial (A) and later (B) oxidation stages.

Temporal dependency of the surface and metal–oxide interface concentrations and potential (C). $\beta = 0.02$ and $\bar{D} = 10$. Same parameters as in Figure 2.

When $(1 - \xi^0_{ox}) < \Lambda$, the electric potentials at the surface and the shrinking core are essentially equal. The smaller the value of β, the higher the electric potential (Figures 3A and 4C). When $\beta \ll 1$ and $\bar{D}\beta \ll 1$, the charge carriers reach the shrinking metal core after a lengthy induction time that increases with decreasing β (Figures 3B and 4C). The carrier concentrations rapidly approach the equilibrium values on both the pellet surface and the shrinking metal core (Figure 4C). A small initial difference between the surface positive and negative charge carrier concentrations rapidly declines (Figure 4C). The negative electric potential increases sharply and monotonously during this initial period. It reaches an asymptotic value after the difference between the concentrations of the two charge carriers vanishes (Figure 4C).

The effects of the initial oxide shell thickness and the Debye screening length are shown in Figures 5–7. When the initial

oxide shell is much larger than the diffusion length, $(1 - \xi^0_{ox}) \gg \sqrt{\tau}$, the surface charge carrier concentrations increase faster the thicker the initial oxide shell thickness is (Figure 5A). A convex carrier distribution forms initially (Figure 5A, $\tau \leq 0.01$). The charge carrier profile later becomes concave and convex again after the metal consumption is complete ($\tau > 0.51$, Figure 5B). For $\beta \ll 1$, a diffusion layer forms with a large difference in the carrier concentrations between the pellet surface and metal interface (Figures 5A and B).

When the initial oxide shell and the Debye screening length are about equal, an essentially uniform electric potential exists in the pellet during its combustion and increases monotonously with time (Figure 6A). The evolution of the charge carrier concentrations and potential on the pellet surface and metal–oxide interface is similar to that with a very thin initial oxide shell, as evident from Figures 4C and 6B.

When $(1 - \xi^0_{ox}) \gg \Lambda$, adjacent regions with positive and negative electric potential coexist initially within the oxide shell; that is, a bipolar electric potential distribution forms initially in the pellet (Figure 7A). The metal oxide interface potential $\phi(i)$ is initially positive then becomes negative (Figure 7B). A transition from bipolar to equipotential electric distribution occurs as the potential vanishes at the metal–oxide

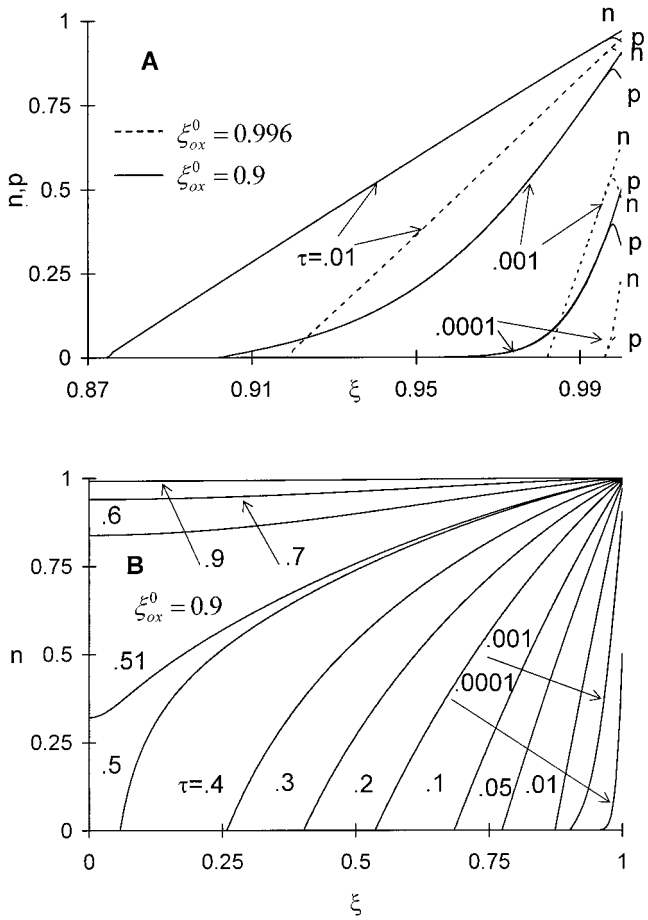

Figure 5. Spatial carrier distributions during the initial (A) and later (B) oxidation stages.

$\xi^0_{ox} = 0.996$ (A) and $\xi^0_{ox} = 0.9$ (A, B). All other parameters are the same as in Figure 4.

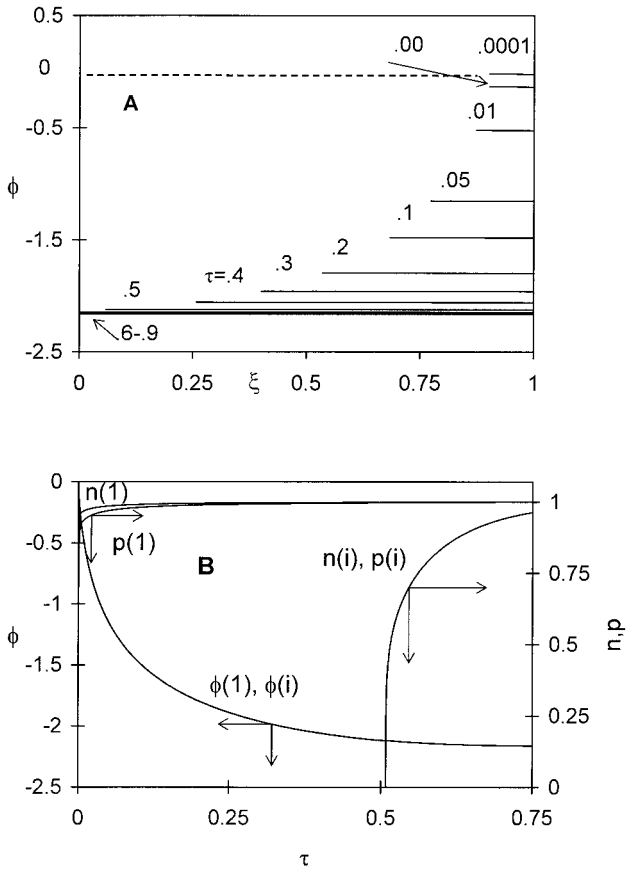

Figure 6. Spatial distribution of the electric potential (A) and temporal dependency of the surface and metal–oxide interface concentrations and potential (B) for the same parameters as in Figure 5B.

interface. The potential difference between the surface and the shrinking metal core decreases as the metal core shrinks (Figure 7A). The thinner the initial oxide shell is, the higher the electric potential (Figures 6B and 7B). The electric potential and electric charge carrier distributions become uniform after complete metal oxidation (Figures 7A and B).

Although the Debye screening length influences the electric potential, it has only a minor impact on the evolution of the carrier concentrations on both the pellet surface and the shrinking metal core. Thus, similar temporal profiles of the charge carriers exist in Figures 6B and 7B, in spite of an order of magnitude difference in Λ. Decreasing Λ decreases the electric potential on both the pellet surface and the metal–oxide interface. The thickness of the initial oxide shell has an opposite impact.

Discussion

Our model assumes that an electric field forms because of the formation of a double-charge layer across a growing MIEC oxide shell as a result of the different diffusivities of oxygen ions (or their vacancies) and electron holes (or electrons). The oxide forms by a very fast chemical reaction at the metal–oxide interface. The model can be readily modified to cases in which

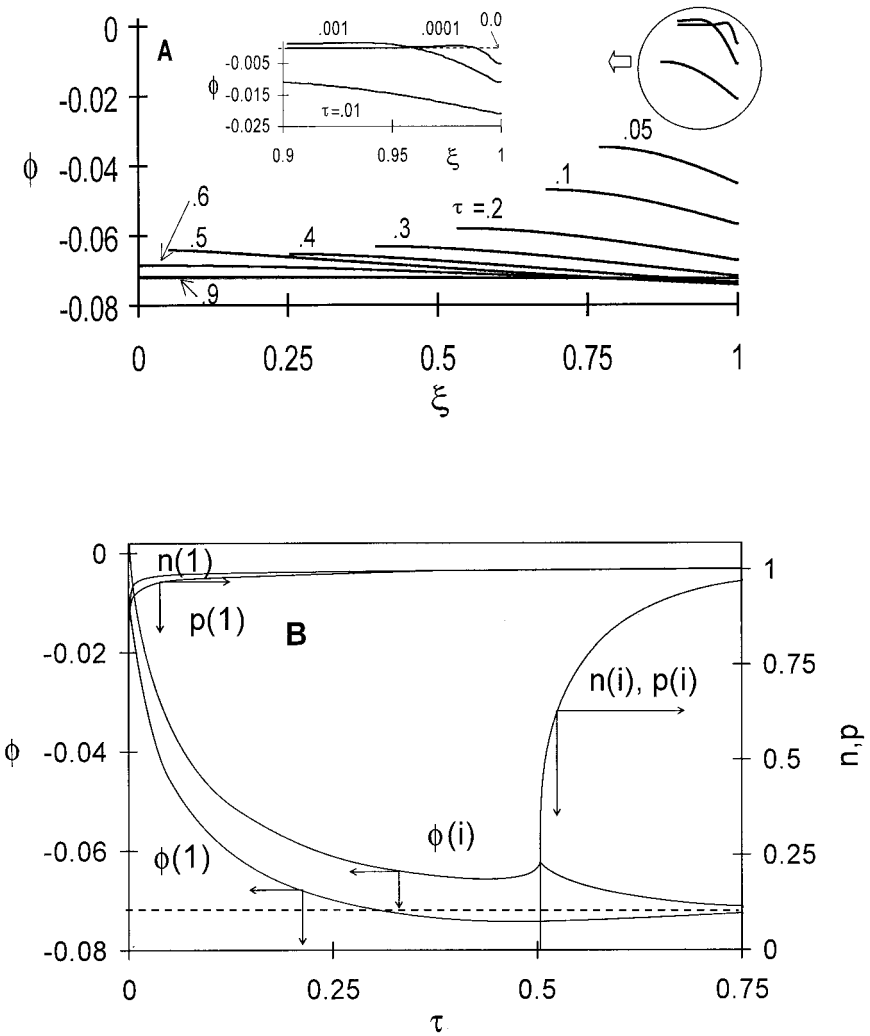

Figure 7. Spatial distribution of the electric potential (A) and temporal dependency of the surface and metal–oxide interface concentrations and potential (B) for $(1 - \xi^0_{ox})/\Lambda = 10$.

Other parameters are the same as in Figure 6.

a semiconductor oxide forms and a reaction between a metal cation and oxygen occurs at the particle surface.

We assumed isothermal particle combustion to decrease the number of parameters in the model. This assumption enhances our ability to determine and focus on the key rate processes and parameters that affect the electrical field formation. The model presented here is just the first step in the analysis of the electrical field generation during metal particle combustion. We currently investigate the impact of the temperature change during the combustion. The results will be presented in a future report.

The presented shrinking core model is valid only when the reaction at the metal–oxide interface (Eq. 4) is much faster than the ion diffusion, that is

$$t_r \ll t_D \tag{31}$$

The characteristic time of the intrinsic metal oxidation (t_r) is of the order of 1 ms at 500°C (Manning et al., 1997). The diffusion time of oxygen atoms at the same temperature in a zirconium oxide shell of $R_0 - R^0_{ox} = 0.1$ μm thickness is

$$t_D \cong (R_0 - R^0_{ox})^2/D_i \cong 4.1 \text{ s}$$

where $D_i = D^0_i \exp(-E/RT)$, $D^0_i \cong 0.018$ cm^2/s, and $E = 131$ kJ/mol (Shelby, 1996).

Thus $t_D/t_r \gg 1$ and this ratio increases with the temperature. The use of the shrinking core model is thus justified because the ratio t_D/t_r is much greater than unity.

Our model does not consider electric potential formation resulting from thermal emission of electrons or chemoionization (gas-phase reactions producing electrons). The electric current formed by the thermoemission and calculated by the Richardson–Dushman equation (Hutchison and Barid, 1963; Kudryashov et al., 1997)

$$I_{el} = BT^2 \exp(-\Phi/kT) \qquad B = 4\pi mek^2/h^3 \tag{32}$$

is much smaller than that measured below 2000°C (Kudryashov et al., 1997; Martirosyan et al., 2003; Morozov et al., 1997; Nersesyan et al., 2002). Data are not available for higher temperatures because they cause melting of the electrodes. Single Ti and Zr particle experiments showed that the maximum voltage was obtained well before the particle attained its maximum temperature and the electric current near the burning particle surface was negligible compared to that on the surface (Martirosyan et al., 2003). If thermal emission or chemoionization had a major impact, the maximum voltage should have been obtained when the maximum temperature is achieved. When the reaction temperature exceeds 2000°C, thermal emission or chemoionization may become a major contributor to the electrical field.

The model assumes that the particle has been rapidly preheated to a temperature at which the formation of the oxide is very fast, so that the reaction proceeds by the shrinking core model. The main advantage of the isothermal model is that it decreases the number of model parameters. This, in turn, enables us to gain an important insight of the rate processes and parameters that have the main impact on the evolution of the electrical field. Some of the parameters in our model are strongly dependent on the temperature. The model does not provide guidance as to which temperature in the large range generated by the combustion should be used. A quantitative prediction of the voltage evolution requires use of a nonisothermal model, which accounts for the variation in the temperature and related parameters. The isothermal model provides insight about the voltage formation and its dependency on the associated parameters.

The predicted profiles of the negative and positive charge carriers are essentially identical, except for initially in the vicinity of the surface. The charge carrier with the larger diffusion coefficient diffuses faster toward the metal core, decreasing its surface concentration. Thus, when the ratio between the positive to the negative diffusion coefficient ($\bar{D}$) exceeds unity, $n > p$ close to the surface, whereas the inverse occurs when $\bar{D} < 1$ (Figures 2A, 2B, 4A, and 5A). As $|\bar{D} - 1|$ increases, the difference in the surface concentration of the two charge carriers increases. This, in turn, increases the surface electric charge and potential. No electric signal forms when the diffusion coefficients are equal. A change in the polarity of the signal may occur if the sign of $\bar{D} - 1$ changes or variation in the ambient oxygen pressure causes the alternative charge carriers to dominate the oxygen transport. Changes in the operating conditions that increase the oxygen adsorption rate (A) increase the surface concentrations of the charge carriers. This, in turn, increases the generated voltage.

The ratio between the characteristic surface molar flux of oxygen ions to the maximum possible flux of oxygen to the pellet surface (β) determines mainly the charge carrier distributions during the later stages of combustion. At low β the carrier flux from the surface is low and the charge carrier surface concentrations grow rapidly after the initiation of combustion (Figures 4B, 6B, and 7B). The charge carriers reach the metal–oxide interface only after a long induction time. Because there is a substantial difference between the surface and interface carrier concentrations, a diffusion layer forms in this case (Figures 4, 6B, and 7B). At high β the flux of the charge carriers is high and they move rapidly toward the pellet center, causing both the surface and interface concentrations to grow slowly (Figure 3B). The difference between the surface and center concentrations decreases with increasing β (Figures 2 and 4).

The oxide shell that forms before the start of the combustion strongly affects the amplitude and dynamic features of the electrical signal. A uniform large electric charge develops inside the whole oxide shell when the initial oxide shell is not thicker than the Debye screening length (Figure 6A). A smaller electric charge develops in a thin surface layer of about the same thickness as the Debye length in pellets with a relatively thick initial oxide shell (Figure 7A). Because the electrical charge is proportional to the volume of this thin surface layer, a higher potential is obtained upon an increase in the Debye screening length. The larger the fraction of the initial oxide shell that is occupied by the Debye screening length, the higher the produced voltage. No electric field forms outside this thin layer. The differences in the surface charge carrier concentrations and the potential increase as the thickness of the initial oxide shell decreases (compare Figures 6A and 7A, 6B and 7B).

When the initial shell is not thicker than the characteristic diffusion and Debye screening lengths, a diffusion layer and nonlinear carrier profiles form only after the growing oxide layer thickness becomes comparable with the diffusion characteristic length (Figure 4B). Because of the small difference in the surface positive and negative carrier concentrations established by that time, the potential in the oxide shell remains uniform and attains a high value as the oxide shell thickness exceeds the Debye screening length (Figure 4C).

When a thick oxide shell exists before the start of the combustion, a small, bipolar electric potential forms initially within the oxide shell (Figure 7A). An excess of the slow diffusing charge carrier exists on the particle surface, whereas an excess of the fast diffusing one develops on the metal–oxide interface. When the slow diffusing carriers reach the interface, these excesses start to diminish, causing a transition to an equipotential distribution. The shift from an excess of fast to slow diffusing charge carriers on the metal–oxide interface causes a switch in the polarity of electric potential on the metal–oxide interface.

Conclusions

Different rates of diffusion of electric charge carriers into a growing MIEC oxide shell can generate an electric potential during the oxidation of a single metal particle. The particle surface and the shrinking metal core surface act as a source and sink of the charge carriers, whereas the MIEC oxide shell separates the charges.

The carrier with the smaller diffusion coefficient determines the sign of the voltage in pellets with a sufficiently thin initial oxide shell (or without it). The larger the difference between the diffusion coefficients, the greater the voltage. The difference in the diffusion coefficients affects the carrier concentrations during a short initial period.

The characteristic surface molar flux of oxygen ions affects the combustion time and the carrier distributions mainly during the later stages of oxidation. A decrease of the flux increases the maximum electric potential and the combustion duration. When the flux is small, a large difference exists between the

carrier concentration at the surface and the shrinking core during most of the combustion.

The thickness of the oxide shell, which formed before the reaction start, has a major impact on the signal shape and amplitude. The thinner this initial shell is, the larger is the voltage amplitude. A unipolar high electric potential forms when the initial oxide shell is thin relative to the Debye screening length. A bipolar potential is predicted to develop when the initial oxide shell is much thicker than the Debye screening length.

Acknowledgments

We are grateful to the National Science Foundation and the Materials Research Science and Engineering Center at the University of Houston for financial support of this research. We thank Dr. S. I. Doronin for help in the numerical calculations.

Notation

Symbols

A	nondimensional oxygen adsorption rate, defined by Eq. 18
$\bar{D}$	ratio between carrier diffusion coefficients, defined by Eq. 21
D_i	diffusion coefficients, m^2/s
e	electron/electron charge, C
h	the Planck's constant, J·s
h^+	electron hole
I	nondimensional maximum oxygen flux, defined by Eq. 29
k	the Boltzmann constant, J/K
k_c	mass transfer coefficients, m/s
m	electronic rest mass, kg
M_W	molecular weight, kg/mol
n	nondimensional concentration of oxygen ions
N_A	Avogadro number
p	nondimensional concentration of electron holes
r	radial coordinate, m
R_0	external radius of spherical particle, m
R_{ox}	shrinking metal core radius, m
T	temperature, K
t	time, s
W_i	surface reaction rates, $mol/(m^2s)$, defined by Eqs. 5–8
y	nondimensional oxygen concentration

Greek letters

β	nondimensional flux of oxygen ions, defined by Eq. 21
ϕ	nondimensional electric potential, defined by Eq. 21
φ	electric potential, V
Φ	work function, eV
Λ	nondimensional Debye screening length, defined by Eq. 22
ν	stoichiometric coefficient
ρ	condensed phase density, kg/m^3
τ	nondimensional time, defined by Eq. 24
ξ	nondimensional radial coordinate, defined by Eq. 21

Subscripts and superscripts

ads	adsorbed
g	gaseous
ox	at the metal–oxide interface
0	initial value
i	interface
$\times$	lattice
*	equilibrium concentrations
∞	ambient conditions

Literature Cited

Ames, W. F., *Numerical Methods for Partial Differential Equations*, 2nd Edition, Academic Press, New York (1977).

Barcilon, V., D.-P. Chen, R. S. Eisenberg, and J. W. Jerome, "Qualitative Properties of Steady-State Poisson–Nernst–Planck Systems: Perturbation and Simulation Study," *SIAM J. Appl. Math.*, **57**(3), 631 (1997).

Chandra, S., *Superionic Solids. Principles and Applications*, North-Holland, Amsterdam, pp. 101–117 (1981).

Dalton, R. C., I. Ahmad, and D. E. Clark, "Combustion Synthesis Using Microwave Energy," *Ceram. Eng. Sci.*, **11**(9–10), 1729 (1990).

Dou, S., C. R. Masson, and P. D. Pacey, "Mechanism of Oxygen Permeation through Lime-Stabilized Zirconia," *J. Electrochem. Soc.*, **132**, 1843 (1985).

Feng, A., and Z. A. Munir, "The Effect of an Electric Field on Self-Sustaining Combustion Synthesis: Part I. Modeling Studies," *Metall. Mater. Trans. B*, **26B**, 581 (1995).

Filimonov, I. A., and N. I. Kidin, "SHS-Process in External Electric Fields," Proc. of 24th Int. Symposium on Combustion, The Combustion Institute, Pittsburgh, PA, 1893 (1992).

Filimonov, I. A., and N. I. Kidin, "Effect of Electric Current on SHS-Process with Complete Transformation in Wave Front," *Combust. Sci. Technol.*, **112**, 15 (1996).

Gellings, P. J., and H. J. M. Bouwmeester, *The CRC Handbook of Solid State Electrochemistry*, CRC Press, New York (1997).

Grigoriev, I. S., and E. Z. Melikhov, *Handbook of Physical Quantities*, CRC Press, New York (1997).

Hutchison, T. S., and D. C. Barid, *The Physics of Engineering Solids*, Wiley, New York (1963).

Jerome, J. W., "Consistency of Semiconductor Modeling: An Existence/Stability Analysis for the Stationary Van Roosbroek System," *SIAM J. Appl. Math.*, **45**(4), 565 (1985).

Kidin, N. I., and I. A. Filimonov, "Self-Propagating High-Temperature Synthesis as a Tool of Composite Material Production under Joule Energy Dissipation," *Mech. Compos. Mater.*, **6**, 1106 (1990) (in Russian).

Kidin, N. I., and I. A. Filimonov, "SHS-Process in an External Electric Field," *Int. J. SHS*, **1**(4), 513 (1992).

Kofstad, P., *High Temperature Corrosion*, Elsevier, London (1988).

Kudryashov, V. A., and A. S. Mukasyan, and I. A. Filimonov, "Chemo-ionization Waves in Heterogeneous Combustion Processes," *J. Mater. Synth. Proc.*, **4**(5), 353 (1997).

Levenspiel, O., *Chemical Reaction Engineering*, Wiley, New York (1962).

Lin, Y.-S., W. Wang, and J. Han, "Oxygen Permeation through Thin Mixed-Conducting Solid Oxide Membranes," *AIChE J.*, **40**(5), 786 (1994).

Maglia, F., U. Anselmi-Tamburini, N. Bertolino, C. Milanese, and Z. A. Munir, "Field Activated Combustion Synthesis of Ta–Si Intermetallic Compounds," *J. Mater. Res.*, **16**(2), 534 (2001).

Manning, P. S., D. S. Sirman, R. A. DeSouza, and J. A. Kilner, "The Kinetics of Oxygen Transport in 9.5 mol % Single Crystal Yttria Stabilized Zirconia," *Solid State Ionics*, **100**, 1 (1997).

Martirosyan, K. S., J. R. Claycomb, G. Gogoshin, R. A. Yarbrough, J. H. Miller, and D. Luss, "Spontaneous Magnetization Generated by Spin, Pulsating and Planar Combustion Synthesis," *J. Appl. Phys.*, **93**(11), 9329 (2003b).

Martirosyan, K. S., I. A. Filimonov, M. D. Nersesyan, and D. Luss, "Electric Field Formation during Combustion of Single Metal Particles," *J. Electrochem. Soc.*, **150**(5), J9 (2003a).

Morozov, Yu. G., M. V. Kuznetsov, M. D. Nersesyan, and A. G. Merzhanov, "Electrochemical Phenomena in the Processes of the SHS," *Dokl. Akad. Nauk RF*, **351**, 780 (1997).

Mrowec, S., *Defects and Diffusion in Solids. An Introduction*, Elsevier, Amsterdam; PWN (Polish Scientific Publishers), Warsaw (1980).

Munir, Z. A., "The Effect of External Electric Fields on the Nature and Properties of Materials Synthesized by Self-Propagating Combustion," *Mater. Sci. Eng.*, **A287**, 125 (2000).

Nersesyan, M. D., J. T. Ritchie, I. A. Filimonov, J. T. Richardson, and D. Luss, "Electric Fields Produced by High-Temperature Metal Oxidation," *J. Electrochem. Soc.*, **149**(1), J11 (2002).

Park, J.-H., and J. W. Jerome, "Qualitative Properties of Steady-State Poisson–Nernst–Planck Systems: Mathematical Study," *SIAM J. Appl. Math.*, **57**(3), 609 (1997).

Press, W. H., B. P. Flannery, S. A. Teukolsky, and W. T. Vetterling, *Numerical Recipes in C: The Art of Scientific Computing*, 2nd Edition, Cambridge University Press, Cambridge, UK (1993).

Ramanarayanan, T. A., S. Ling, and M. P. Anderson, "Electrochemical Analysis of Mixed Conduction in Ceramic Oxide Membranes," Proc. of

the 2nd Int. Symposium on Solid Oxide Fuel Cells, Athens, Greece, pp. 777–786 (1991).
Rode, H., V. Hlavacek, H. J. Viljoen, and G. E. Gatica, "Combustion of Metallic Powders: A Phenomenological Model for the Initiation of Combustion," *Combust. Sci. Technol.*, 88, 153 (1992).
Rode, H., D. Orlicki, and V. Hlavacek, "Reaction Rate Modeling in Non-Catalytic Gas-Solid Systems: Species Transport and Mechanical Stress," *AIChE J.*, **41**(12), 2614 (1995).
Shelby, J. E., *Handbook of Gas Diffusion in Solids and Melts*, The Materials Information Society, ASM International, Materials Park, OH (1996).
Thomas, L. H., *Elliptic Problems in Linear Difference Equations over a Network*, Watson Science Computer Lab. Report, Columbia University, New York (1949).
Trofimov, A. I., and V. I. Yukhvid, "The Effect of an Electromagnetic Field on the Ti+C System," *Fizika Goreniya i Vzryva*, **1**, 71 (1993) (in Russian).
Wen, C. Y., "Noncatalytic Heterogeneous Solid Fluid Reaction Models," *Ind. Eng. Chem.*, **60**(9), 34 (1968).
Zakiev, S. E., "The Effect of Radio Frequency Heating on Self-Propagating High-Temperature Synthesis," *Int. J. SHS*, **8**(1), 1 (1999).

Manuscript received Aug. 15, 2003, and revision received Dec. 20, 2003.